Isomerization of *n*-hexane on Pt–Ni catalysts supported on nanocrystalline H-BEA zeolite

Patrícia M. Lima [a],*, Teresita Garetto [b], Célio L. Cavalcante Jr. [c], Dilson Cardoso [d]

[a] *University of Brasília, Chemistry Institute, 70910-900 Brasília-DF, Brazil*
[b] *Catalysis Science and Engineering Research Group, INCAPE- 3000 Santa Fe, Argentina*
[c] *Federal University of Ceará, Chemical Engineering Department, Fortaleza-CE, Brazil*
[d] *Federal University of São Carlos, Chemical Engineering Department, São Carlos-SP, Brazil*

ARTICLE INFO

ABSTRACT

The zeolite Beta used in this work consists of nanosized crystallites (20–30 nm) aggregates, determined by HRTEM analysis. The influence of the zeolite structure and crystallite size on the desorption rates of linear paraffins was determined by ZLC chromatography. Desorption from Beta zeolite was faster than from USY zeolite. IR acidity analysis by adsorption and desorption of pyridine showed that Beta zeolite has a smaller number of Brønsted acid sites than USY zeolite, but that they are a little stronger. Pt–Ni/H-BEA catalysts showed higher activity than Pt–Ni/H-USY ones. This behavior can be attributed to the very small crystallites of Beta zeolite, which enable faster diffusion of the reactant and products molecules. Among bimetallic catalysts, the highest activity was observed with that containing 60% Pt. This result is very interesting in view of the cost reduction, relative to 100% Pt catalyst.

1. Introduction

The isomerization of alkanes has become increasingly important for the oil refining industry. This reaction transforms straight-chain into branched-chain paraffins, which have higher octane numbers. In this way, pollution caused by the use of lead additives and aromatics in gasoline is reduced. Paraffin isomerization is typically carried out on bifunctional catalysts containing metal sites, for dehydrogenation/hydrogenation steps, and acid sites for skeletal rearrangement. It is well established that high branching is achieved through consecutive isomerization reactions [1–3].

A typical isomerization catalyst is platinum supported on chlorided alumina, which is very active and can be operated at low temperatures. However, this catalyst causes corrosion and pollution and is sensitive to feeding line impurities, such as water and sulfur compounds [4,5]. The use of zeolites as an acidic support can eliminate such problems. Platinum supported on Mordenite zeolite (Pt/H-MOR) has been used commercially for the isomerization of linear alkanes to higher octane branched isomers [6]. This zeolite has strong acidity and is very suitable for these small alkanes giving a high yield of isomers; however, it is less selective when operating with longer chain paraffins. Pt catalysts supported on three-dimensional channels of Beta and USY zeolites were reported to have higher selectivity and activity than one-dimensional Pt/H-MOR in the isomerization of *n*-C$_7$ and *n*-C$_8$ paraffins [7–11].

Platinum is by far the best studied metal in catalysts for this type of reaction, because of its high activity and stability. However, platinum is expensive and it would be interesting to use cheaper catalysts with the same or better catalytic properties. Recent studies on Pt–Ni bimetallic systems supported on H-USY zeolite [12–14] showed that these provided catalytic activity equal to or higher than that of monometallic Pt catalysts.

On the other hand, it has been reported that, in the isomerization of *n*-alkanes, Pt/H-BEA catalysts have higher activity and selectivity than Pt/H-Y [10,15,16]. The authors suggest that such behavior is related to the stronger acidity of the Pt/H-BEA catalysts. These conclusions are based on infrared spectroscopy (IR) of the adsorption of pyridine [15] and temperature-programmed desorption of pyridine [10,16].

In this context, many studies [10,15,16] show the high potentiality of Beta zeolite. However, little information has been gained on the features responsible for the high activity of this zeolite. As a result, this study had the objective of preparing bifunctional catalysts containing Pt and Ni supported on Beta zeolite and testing these catalysts in the reaction of *n*-hexane isomerization. Additionally, the properties of Beta zeolite and the supported catalysts were characterized by various techniques, to gather information (sorption kinetics, quantity and strength of acid sites, reduction properties and metal dispersion) that could explain better their high catalytic activity.

---

* Corresponding author. Tel.: +55 61 31073819; fax: +55 61 31070780.
E-mail address: patricialima@unb.br (P.M. Lima).

2. Experimental

2.1. Catalyst preparation

The catalysts were prepared from an ammonium form (NH_4-BEA) of Beta zeolite (CP-814N), commercially available from Zeolyst with an overall Si/Al ratio of 9:1. H-USY zeolite supplied by Engelhard (EZ-190P), with an overall Si/Al ratio of 6:1, was used for comparison with H-BEA catalysts. The framework of H-USY zeolite has a Si/Al ratio of 11:1, calculated from X-ray diffraction (XRD) and magic angle spinning nuclear magnetic resonance of ^{29}Si (^{29}Si MAS-NMR) data [12]. In order to remove any Al^{+3} or H^+ ions present in the commercial zeolites, and to transform them fully to the ammonium form, they were exchanged three times with a 1 M NH_4Cl aqueous solution and then washed until no Cl^- was detected in the filtrate. The precursors of the Ni and Pt cations were their ammine complex chlorides $[Ni(NH_3)_6]Cl_2$ and $[Pt(NH_3)_4]Cl_2$. The platinum salt was commercially available from Aldrich and the nickel complex was synthesized by the method suggested by Brauer [17].

The method used to achieve a uniform distribution of the cations in the zeolite crystals was competitive ion exchange [18], with a competition ratio $NH_4^+/Ni^{2+} = 20$ and $NH_4^+/Pt^{2+} = 10$ [19]. An aqueous solution of the metallic precursors containing the required amount of NH_4Cl was added gradually to a zeolite suspension in water and then stirred for 5 h at room temperature ($\sim25\,^\circ C$). For the Beta zeolite, in order to achieve better ion exchange efficiency with the transition metal cations, the ion exchange was performed at pH 10, achieved by adding NH_4OH solution (2.5 M). The resulting solution was filtered and washed to eliminate Cl^- ions. The exchange efficiency of the transition metal cations was estimated by analyzing the filtrate using inductively coupled plasma spectroscopy (ICP), and in all samples the efficiency was approximately 100%. In view of the large difference between the atomic masses of Ni and Pt, the metal contents of the Pt–Ni bimetallic catalysts are reported here in micromol units per gram of catalyst [13,14] rather than mass %, and range from 80 to 230 μmol metal/g_{cat}.

With the aim of obtaining the catalysts in the proton form, after ion exchange, these precursors obtained were calcined under a flow of air (100 mL min^{-1} $g_{cat}$$^{-1}$), at a heating rate of 2 $^\circ$C min^{-1} up to 500 $^\circ$C and kept at this temperature for 2 h. The activation of the catalysts was then performed *in situ*, using the 'fast activation' method [13,14]. This process consisted of heating samples under fast-flowing hydrogen (2 L min^{-1} $g_{cat}$$^{-1}$) and at a rapid temperature ramp (30 $^\circ$C min^{-1}) up to various final temperatures (from 350 to 550 $^\circ$C), and at which they are kept for short times (5, 30 or 60 min). For the purpose of comparison, the 'traditional activation' method [14] was also used, which involves heating the sample at a slow rate (2 $^\circ$C min^{-1}), under a slower flow of hydrogen (1 L min^{-1} $g_{cat}$$^{-1}$), up to 500 $^\circ$C and maintaining this temperature for 6 h.

2.2. Characterization of Beta zeolite

The framework Si/Al ratio of commercially available Beta zeolite (CP-814N) was analyzed by ^{29}Si MAS NMR technique. The solid state ^{29}Si MAS NMR spectra were recorded at ^{29}Si frequency of 79.2 MHz and a sample spinning rate of 3 KHz on a Varian Infinity Plus-400 spectrometer. XRD analysis was used to confirm the BEA phase of commercially available Beta zeolite, with a Rigaku X-ray diffractometer, DMax 2500PC, using Cu-K$_\alpha$ radiation (λ = 1.54 Å) in the scan range 2θ from 5 to 45°, at a scan rate of 0.5° min^{-1}. The average diameter of Beta zeolite crystals was determined from the value of the half-height width (B = 0.63°) of the most intense peak (2θ = 22.4°), using the Scherrer equation [20,21]. The particle and crystallite dimensions of Beta zeolite

were also determined with a scanning electron microscope (HRSEM JEOL JSM-6700F) or a transmission electron microscope (HRTEM JEOL JEM-2100F), both providing high resolution: 1.0 and 0.17 nm, respectively.

Textural properties of Beta zeolite were measured by nitrogen adsorption at $-196\,^\circ$C on an ASAP-2400 analyzer (Micromeritics), after the sample was pretreated at 200 $^\circ$C under vacuum for 2 h. The acidity of the samples was assessed by IR, after adsorption of pyridine and desorption at three different temperatures (150, 250 and 350 $^\circ$C) on Nicolet 760 FTIR equipment. The band areas of the adsorbed pyridine were calculated with the Nicolet software package OMNIC, using a constant mass of 10 mg for the zeolites. The band area related to Brønsted sites was calculated between wave numbers 1565 and 1510 cm^{-1}, while those related to Lewis sites were calculated between wave numbers 1470 and 1420 cm^{-1}. The sorption kinetics of *n*-alkanes on Beta zeolite was determined by zero length column chromatography (ZLC), as detailed in a previous study [22].

2.3. Characterization of the catalysts and precursors

Samples containing Ni and Pt cations were characterized by temperature-programmed reduction (TPR), carried out on a Micromeritics Pulse Chemisorb 2705 system provided with a thermal conductivity detector (TCD) to monitor H_2 consumption. Before the TPR run, the sample (100 mg) packed in a quartz U-tube was heated under flowing nitrogen up to 200 $^\circ$C at 10 $^\circ$C min^{-1} held there for 1 h, and then cooled down to 25 $^\circ$C. A reducing gas, 5% H_2/N_2, was allowed to flow through the reactor at a rate of 30 mL min^{-1}. The TPR was then carried out by heating the reactor up to 1000 $^\circ$C at a continuous rate of 10 $^\circ$C min^{-1}. The TPR was also performed after samples were reduced by the 'fast activation' method at various final temperatures for 30 min, in order to analyze the proportion of unreduced cations remaining after activation.

The metallic dispersion of the catalysts was assessed by the hydrogen chemisorption technique. The analysis was carried out with a Micromeritics Autochem II 2920 Automated Catalyst Characterization System. Before analysis, the calcined precursors were reduced by 'fast activation' at various final temperatures for 30 min. For the purpose of comparison, the 'traditional activation' method was also employed. The reduction conditions were the same as those used to activate the catalysts before the reaction. After reduction, the catalysts were cooled down in argon flowing at 70 mL min^{-1}. Chemisorption was carried out at 40 $^\circ$C with 0.5 mL pulses of 5% hydrogen in argon, repeatedly injected until no further hydrogen was chemisorbed. The total volume of chemisorbed H_2 was estimated by adding the fraction of H_2 consumed in each pulse.

2.4. Catalytic experiments

Isomerization of *n*-hexane was carried out in a continuous fixed-bed reactor, under atmospheric pressure and at 230 $^\circ$C, with a molar ratio of H_2/*n*-C_6 = 9.0 in the feed. *n*-Hexane was fed into the reactor with a syringe pump with a rate of 2 mL h^{-1}, while hydrogen flowed at 55 mL min^{-1}. A mass of 50 mg Pt–Ni/HBEA catalysts was used, corresponding to a W/F$_{n\text{-}C6}$ contact time of about 2.28 min. The mass of Pt–Ni/HUSY catalysts, used for comparison, was 100 mg, corresponding to a W/F contact time of about 4.56 min. The calcined catalyst precursors were reduced *in situ*, using the activation conditions detailed above. Products from the reaction were analyzed on a VARIAN Star 3400 gas chromatograph equipped with a LM-1 capillary column (50 m and 0.25 mm i.d.) and a flame ionization detector (FID).
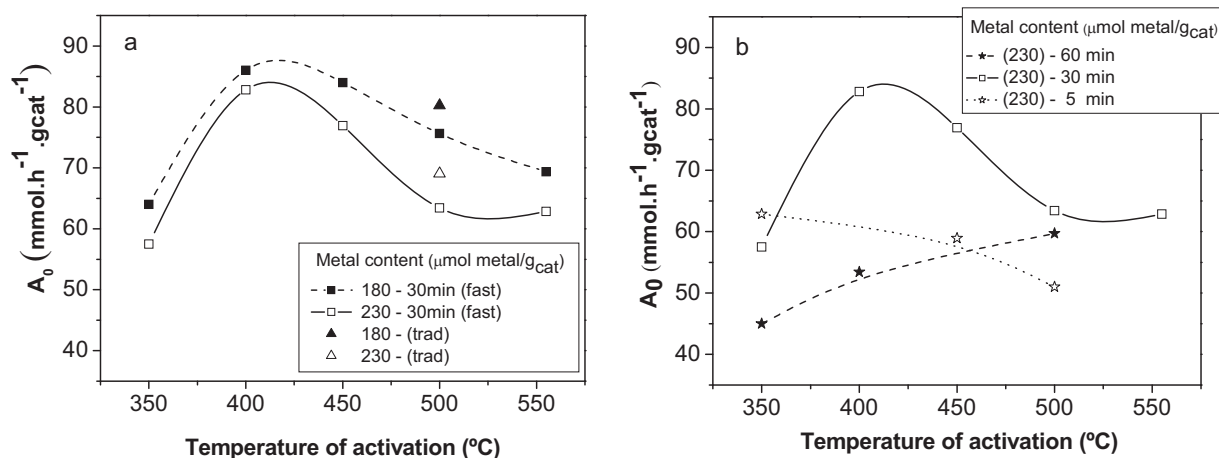
Fig. 1. Variation of initial isomerization activity (A_0) of 60Pt/H-BEA catalysts with activation temperature and (a) activation method and metal content, (b) fast activation time.

3. Results and discussion

3.1. Catalytic tests

Fig. 1a shows the results for initial isomerization activity (A_0) of catalyst 60Pt/H-BEA, containing 180 and 230 μmol Metal g_{cat}^{-1}, reduced with the 'fast activation' method for 30 min. A second order exponential decay function was fitted to the experimental data [12,14], and the adjusted curves were extrapolated to zero time of reaction to obtain the initial activity (A_0). For both metal contents, the highest values of initial activity were achieved with catalysts reduced at temperatures of 400 and 450 °C. However, the activity decreased slightly as metal content increased. For activation temperatures below this range, the activity is lower, probably due to an incomplete reduction of the transition metal cations. Catalysts activated above 450 °C also showed lower activity probably because the metallic particles were sintered, decreasing the dispersion of the active metal over the surface. Fig. 1a also shows that, for the catalysts containing 180 and 230 μmol Metal g_{cat}^{-1}, the values of initial activity achieved by the 'traditional activation' method at 500 °C (indicated by triangles) were close to those achieved by the 'fast activation' at the same final temperature. However, the activities achieved at 400 and 450 °C by the 'fast activation' method were significantly higher than those achieved by the traditional method. In this regard, the 'fast activation' method is quite advantageous, especially in view of the speed of this process.

The influence of the reduction time on the initial activity, when the 'fast activation' was used, for the catalyst containing 230 μmol Metal g_{cat}^{-1}, can been seen in Fig. 1b. Catalysts reduced for 5 min had activities lower than those reduced for 30 min, probably due to incomplete reduction of the transition cations. The samples reduced for 1 h also had lower activities than samples that were reduced for 30 min. As will be seen from the characterization of these catalysts, the activity fell during the 1 h reduction due to the sintering of metal particles, promoted by the higher reduction temperature.

Fig. 2 shows the variation of the initial isomerization activity with the percentage of platinum, for catalysts with various total metal contents. In light of the results showed in Fig. 1, these catalysts were reduced by 'fast activation' at 450 °C for 30 min. It can be seen that for all the catalysts, the initial activity increases with Pt content up to a 60% in the bimetallic catalysts. It is interesting to note that, at the higher Pt proportions, the catalyst activity equaled that of the monometallic platinum catalyst.

These results are encouraging when the cost reductions achieved by substituting bimetallic catalysts for monometallic Pt catalysts are calculated. Similar behavior was also observed in our previous studies [12–14] with bimetallic catalysts supported on USY zeolite. Jordão et al. [12] revealed by HRTEM analysis that the metal particles of the bimetallic catalysts were smaller than the monometallic catalyst particles of platinum. Therefore, it seems that the addition of Ni can prevent the aggregation or sintering of platinum particles, thus increasing the dispersion of the metal. The activity decreases with higher metal content, as a consequence of the diminution of metal dispersion (see Fig. 9).

Fig. 2 also compares the initial activity of catalysts supported on H-USY, with those supported on H-BEA, under the same reaction conditions. It is noteworthy that the activities of the H-BEA catalysts were significantly higher than those supported on zeolite H-USY.

Fig. 3 shows the initial selectivity for bi-branched isomers, which have the highest octane number among the products, against the percentage of platinum in Pt–Ni/H-BEA catalysts. For all Pt–Ni/H-BEA catalysts, the conversion to *n*-hexane isomers was above 98%. Consequently, the difference from 100% selectivity belongs to cracking products. The selectivity for bi-branched isomers decreases slightly from 12 to 8% as the platinum percentage increases, and changes insignificantly with the total metal content.
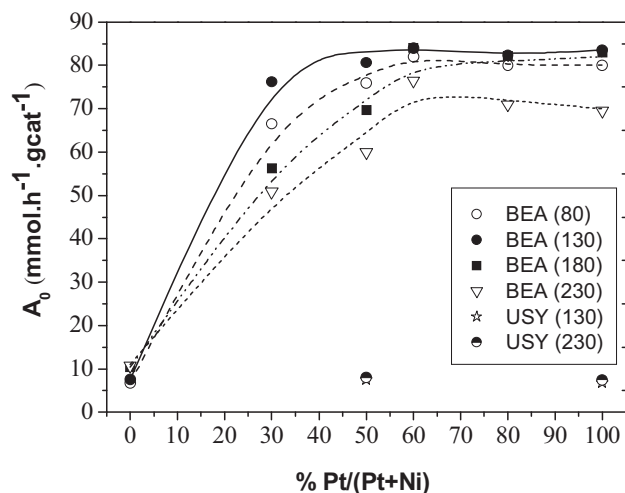

Fig. 2. Initial activity (A_0) of Pt–Ni/H-BEA and Pt–Ni/H-USY catalysts, with various metal contents and Pt proportions, activated by 'fast activation' for 30 min at 450 °C.
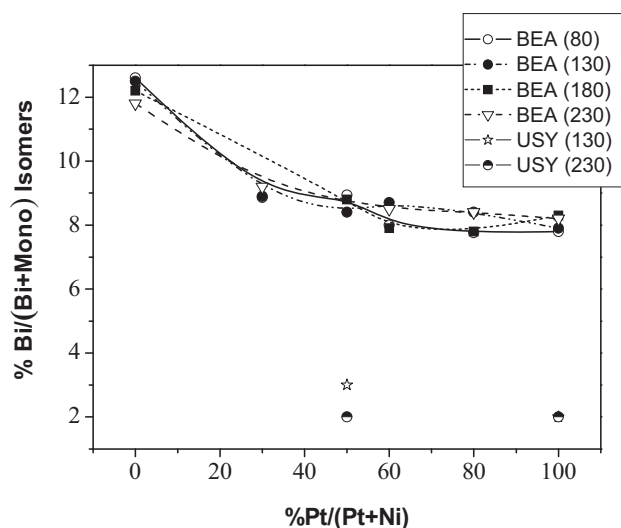
Fig. 3. Selectivity for bi-branched isomers of Pt–Ni/HBEA and Pt–Ni/HUSY catalysts with various total metal contents, as a function of platinum proportion.

This suggests that the metal content is not the rate-determining factor for the formation of these products, but rather the number of Brønsted acid sites, which remains constant in these catalysts. Besides, from Fig. 3 it can also be seen that the selectivity to bi-branched isomers of Pt–Ni/H-BEA catalysts was significantly higher than that of Pt–Ni/H-USY ones. This is a consequence of the much higher activity of the catalysts, which also enhances the formation of these secondary isomerization products. Then, when both catalysts are compared in the same reaction conditions, the yield to bi-branched isomers is significantly higher with Pt–Ni/H-BEA catalysts due its higher conversion. The high yield of a desired product is very important in the industry.

3.2. Characterization of BEA zeolite

The XRD pattern of commercially available CP-814N zeolite showed the most intense diffraction peaks in the $2\theta = 20$–$32°$ region and corroborated the BEA structure [23]. The average diameter of the crystallites, estimated with the Scherrer equation, was approximately 14 nm. This result shows that the NH$_4$-BEA is a nanocrystalline zeolite, as found by Camblor et al. [24] in Beta zeolites synthesized with various Si/Al ratios.

The Si/Al ratio of the NH$_4$-BEA zeolite framework, analyzed by ^{29}Si MAS NMR was 9.6, very close to the global Si/Al ratio provided by the manufacturer (Si/Al $_{global}$ = 9.0). This result shows that most of the aluminum is located in the framework of this zeolite. Actually, ^{27}Al MAS NMR shows an intense signal of tetrahedral coordination (framework) and also the presence of some extraframework octahedral aluminum. However, the quantitative MAS NMR analysis for this element is somewhat difficult [25].

High-resolution scanning electron microscopy (HRSEM) analysis shows that grains of NH$_4$-BEA zeolite are formed by aggregates of particles of indefinite form, 100–200 nm in size (Fig. 4a). HRTEM micrographs of these particles, as in Fig. 4b, show that they consist of crystallites between 20 and 30 nm, some of them with an octahedral form, typical of Beta zeolite [26]. This result is very close to the average diameter of 14 nm estimated by XRD analysis of 14 nm. By contrast, the USY zeolite under study has significantly bigger crystals (800 nm) [27].

The nitrogen adsorption isotherms of zeolites NH$_4$-BEA (Fig. 5a) and H-USY (Fig. 5b) are typical of microporous materials that have a high adsorption capacity at very low pressures. In addition, as the nitrogen pressure increases (indicated by an arrow), Beta zeolite continues adsorbing up to a value of 310 cm^3 g^{-1}. On the other hand, the adsorption on H-USY zeolite remains practically constant (characteristic of a BET isotherm Type I), reaching a value of 200 cm^3 g^{-1}, much lower than that seen in Beta zeolite. This is due to the external surface area of the Beta zeolite being higher than that of USY (see Table 1), as a result of the much smaller crystallites in the former. Moreover, the adsorption isotherm of Beta zeolite has a hysteresis loop, indicating the presence of interparticle mesopores created by the aggregation of the small crystallites (Fig. 4b).

Table 2 shows the values of areas calculated from the integrated IR absorbance bands attributed to pyridine adsorbed on Brønsted and Lewis zeolite acid sites. It can be observed that at all temperatures, USY zeolite (Si/Al = 11.0) has a higher intensity of Brønsted bands than BEA zeolite (Si/Al = 9.0), suggesting that the Beta zeolite has a lower density of Brønsted sites than USY. This is probably due to the higher number of defects present in this zeolite, related to its very small crystals. Considering that the Si/Al ratio of both zeolites is comparable, this supposition is supported by the higher density of Lewis sites observed in the Beta zeolite, as shown in Table 2. The strength of Brønsted sites can be estimated from the slope of the curves (Table 2) of the amount of pyridine desorbed as a function of temperature, between 150 and 350 °C. The higher the absolute value of these slopes, the higher the rate of pyridine desorption
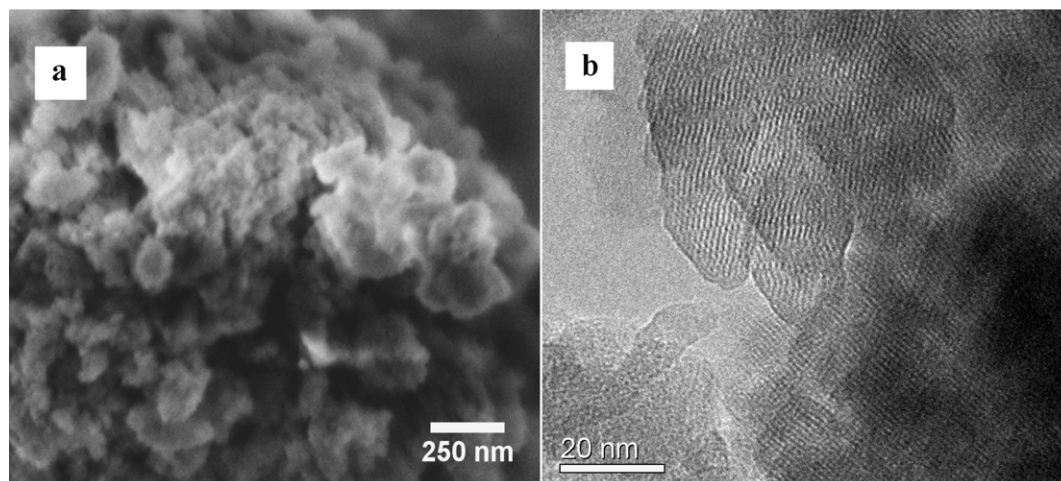

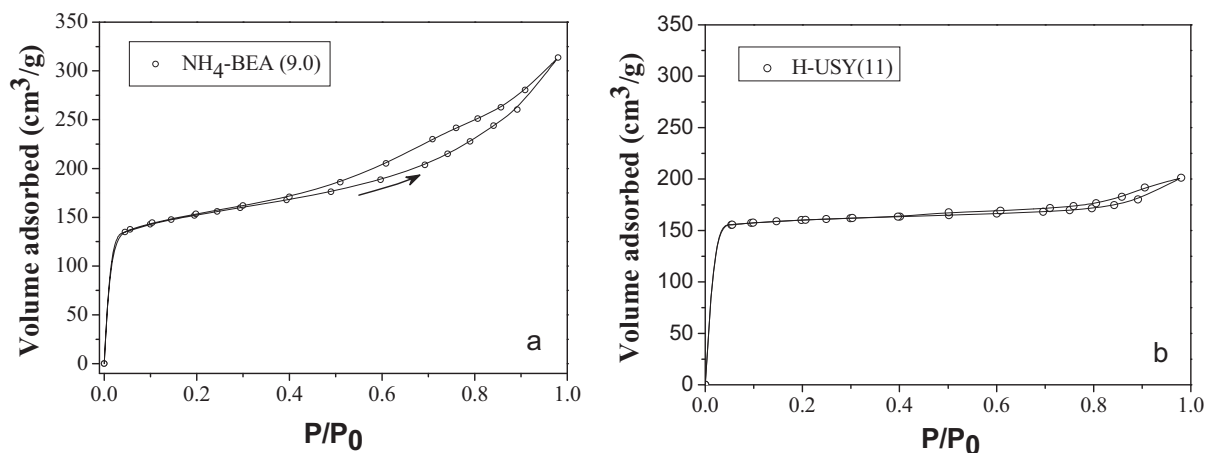**Fig. 4.** (a) HRSEM and (b) HRTEM micrographs of NH$_4$-Beta zeolite.

Fig. 5. The isotherm of N_2 adsorption on zeolites, (a) NH_4-BEA and (b) H-USY.

Table 1
Textural properties of NH_4-BEA and H-USY zeolites.

Zeolite	External surface area ($m^2\,g^{-1}$)[a]	Micropore volume ($cm^3\,g^{-1}$)[b]	Average diameter of crystallites (nm)[c]	Crystallite diameter (nm)
NH_4-BEA	214.4	0.14	14	20–30[d]
H-USY	57.8	0.22	–	800[e] [26]

[a] Calculated from the BET external surface area.
[b] From t-plot method.
[c] Determined by XRD technique.
[d] Determined by HRTEM technique.
[e] Determined by SEM technique.

with increasing temperature and, therefore, the higher the density of weak sites present in the zeolite. If the valor of the slope is near zero, it means the sites are very strong. From the slope results, it can be concluded that the H-BEA zeolite has stronger Brønsted acid sites than H-USY zeolite, but the difference is not very significant.

The desorption of n-decane from zeolite H-BEA was measured in order to study the alkane diffusion kinetics. It was not possible to measure the desorption of n-hexane in zeolite BEA because the diffusion of this smaller molecule was so fast to be detected. In Fig. 6a, this curve is compared to that obtained using H-USY zeolite [27], showing that desorption is much faster in Beta zeolite than in USY. For example, in zeolite H-BEA, C/C_0 decreases to 10% of its original value in approximately 25 s, while in H-USY, this drop was much slower, taking about 250 s. Although these zeolites have different channels sizes, they have very similar micropore diameters (0.74 nm in structure FAU and 0.67 nm in BEA). However, the diffusion path in Beta zeolite is very short, because its crystallites are much smaller (14 nm) than the 800 nm reported for the USY zeolite crystallites [27].

Fig. 6b shows another significant feature of both zeolites: the desorption rate of n-decane, determined by differentiating the curves seen in Fig. 6a. While the initial desorption rate of n-decane from H-BEA is very high and decreases with time, the initial desorption rate from H-USY is nearly zero, rising a maximum, which is much smaller than the initial desorption rate of H-BEA. This initial delay in desorption of n-decane from zeolite H-USY is probably due to the large sizes of the crystallites of this material.

Table 2
Integrated absorbance of the IR-bands attributed to the pyridine adsorbed in Brønsted and Lewis acid sites of the zeolites.

Catalysts	Brønsted			Slope ($\times 10^4$)	Lewis		
	150 °C	250 °C	350 °C		150 °C	250 °C	350 °C
BEA(9)	3.00	2.05	0.82	−109	4.56	3.63	3.00
USY(11)	4.86	3.89	1.92	−147	4.74	3.15	2.26

Therefore, the better catalytic performance of the Pt–Ni/H-BEA catalysts seen in Fig. 2 can be explained by the very small size of their crystals (14 nm). This can improve the diffusion of reactant and products. Chica and Corma [11] observed that the activity of the nanocrystalline zeolite BEA (30 nm) in the n-octane isomerization was significantly higher when compared with a zeolite BEA with bigger crystals (1000 nm). In addition, since Beta zeolite crystallites are very small, their large external surface (Table 1) probably exposes a high number of external active sites, enhancing the isomerization reaction [21]. Since, the strength of the acid sites of zeolite H-BEA is not very different when compared with zeolite USY (Table 2), the crystal size seems to be a determinant factor to explain the difference of activity catalytic between these zeolites. Further, a study using a nanocrystalline zeolite USY had to be made to conclude the influence the crystal size in the n-alkanes isomerization.

3.3. Characterization of the precursors and catalysts

Fig. 7 shows the TPR profiles obtained from BEA catalysts containing 180 μmol Metal g_{cat}^{-1}: monometallic nickel, monometallic platinum and the bimetallic 60Pt/H-BEA catalyst, which presented the highest activity. The nickel monometallic catalyst (curve a) showed two reduction peaks at 445 and 555 °C (γ and δ, respectively). The platinum monometallic catalyst (curve c) also presented two reduction peaks but, as a result of the easier reducibility of the Pt^{2+} cations, they appeared at lower temperatures: 190 and 390 °C (α and β, respectively). However, in the bimetallic catalyst containing 60% Pt (curve b), the Ni^{+2} reduction peak at 550 °C (δ) disappeared and the intensity of the peak around 400 °C was enhanced. Possibly the hydrogen consumption of this latter peak is due to the sum of the species responsible for peaks β, γ and δ. Such behavior of bimetallic precursors is explained by Jao et al. [28] in two ways: (1) since the Pt^{2+} cations are reduced before the Ni^{+2}, the resulting metallic platinum generates active
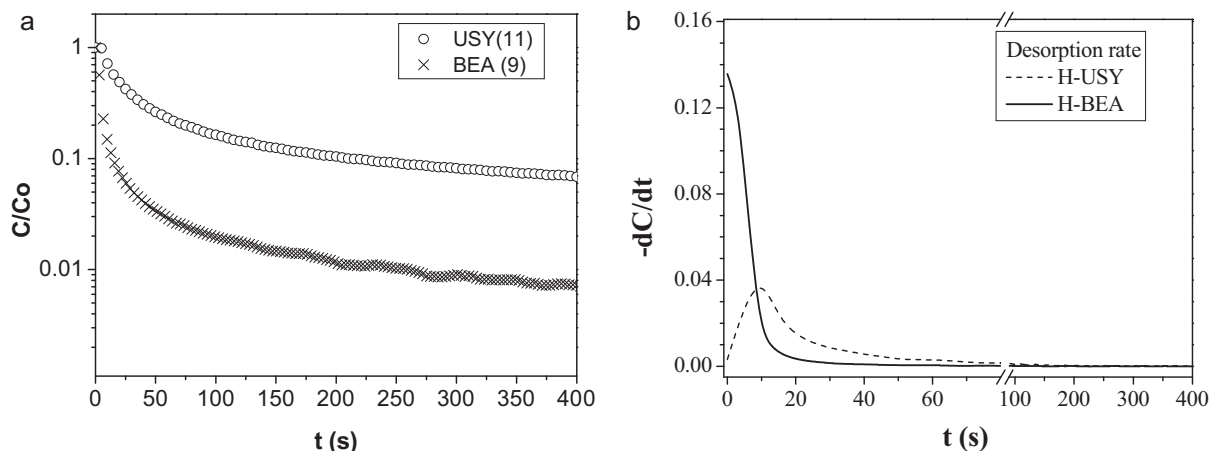
Fig. 6. (a) Desorption curves for *n*-decane in Beta and USY zeolites at 150 °C at purge flow rate of 40 mL/min (b). Desorption rates obtained by differentiating curves in (a).

sites required for the dissociation of hydrogen, thus enabling the reduction of Ni^{+2} in the bimetallic catalysts; (2) another way to explain the shift of Ni reduction to a lower temperature in Pt–Ni catalysts is by hydrogen spillover from the reduced Pt to the nickel oxide.

Jordão et al. [12] attributed the various reduction peaks obtained with Ni/H-USY catalysts to different positions of the cations in this zeolite, ascribed by Suzuki et al. [29] as α (large cavity), β (sodalite cavity) and γ (hexagonal prisms). Those authors found that the reduction temperature of the Ni^{2+} cations located in the α-, β- and γ-positions increased in this order. Similar remarks were made by Tzou et al. [30] about the reduction peaks of Pt/H-USY catalysts.

However, differently from the USY structure, Beta zeolite is not formed by cavities; its structure consists of a three-dimensional channel system. For example, Ho et al. [31] studied the reduction of PtO supported on pure silica and Pt^{+2} cations in exchangeable positions in H-Beta zeolites with various Si/Al ratios. In the Beta zeolite with Si/Al = 11, they found two important peaks, one at −50 °C, attributed to the easy reduction of PtO at the surface in a H_2 atmosphere. The major peak, at 430 °C, was attributed to the reduction of Pt^{+2} cations coordinated with siloxy anions $[SiO_4^-]$, which are in large amounts present in Beta zeolite. Ho et al. [31] also found two minor peaks at 80 °C and 250 °C; in view of the results from Ostgard et al. [32], they were attributed to PtO occluded in channels and Pt^{+2} cations, respectively.

In our case, according to Ostgard et al. [32], the α peak seen at lower temperature (190 °C, curve c in Fig. 7) can be attributed to the reduction of Pt^{2+} cations compensating framework tetrahedral anions (AlO_4^-). Also, the TPR β peak observed at 390 °C with the Pt/H-BEA catalyst (curve c in Fig. 7), in agreement with Ho et al. [31], can be attributed to a reduction of stable species formed by the coordination of the Pt^{2+} cations with siloxy anions $[SiO_4^-]$. Ho et al. [31] consider that these species may interact strongly with the Beta zeolite, which would explain the very high reduction temperature of these Pt cations.

For the Ni/H-BEA TPR results (curve a in Fig. 7) similar attributions may be made for the two reduction peaks (γ and δ). The first (at 445 °C) can be attributed to the reduction of Ni^{2+} cations compensating framework tetrahedral anions (AlO_4^-) and the latter (at 555 °C) to a reduction of stable species formed by the coordination of Ni^{2+} cations with siloxy anions $[SiO_4^-]$.

Fig. 8 shows TPR profiles obtained from the 60Pt/H-BEA bimetallic catalyst after its 'fast activation' by reduction for 30 min at 350 °C (curve b) and 400 °C (curve c), as well as the original profile (curve a), equivalent to Fig. 7, curve b. The numbers inserted in Fig. 8 represent the areas under the curves and they are proportional to the hydrogen consumption during the reduction of the cations (a) in the original sample and (b) and (c) that remained after the 'fast activation'. It can be seen that, after the catalyst activation at 350 °C, there is a significant decrease in the hydrogen consumption, compared
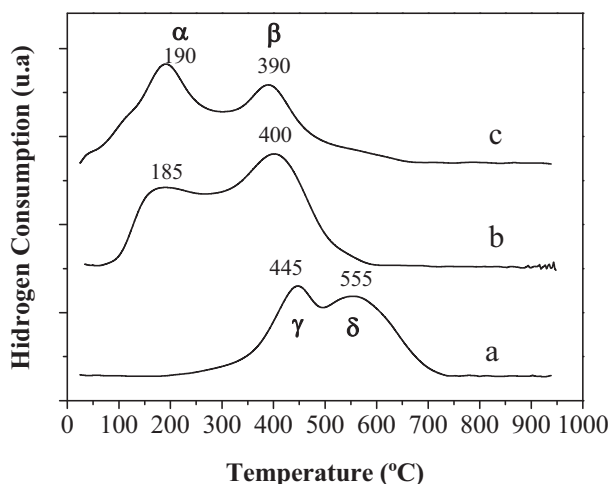

Fig. 7. TPR of Pt–Ni/H-BEA catalysts containing 180 μmol Metal g_{cat}^{-1}: (a) 100% Ni, (b) 60% Pt 40% Ni and (c) 100% Pt.
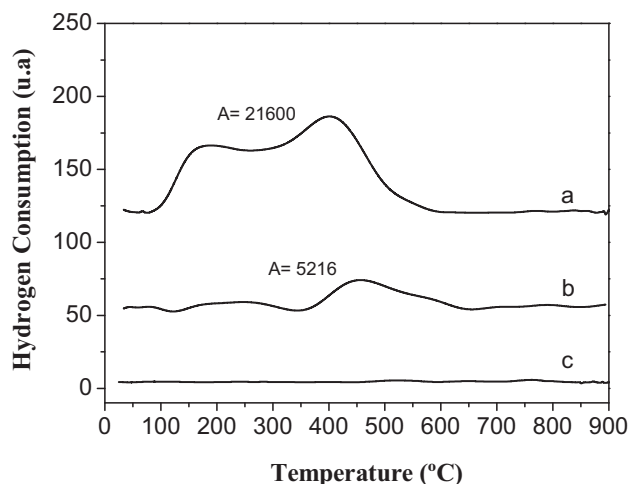

Fig. 8. TPR of 60Pt/H-BEA catalyst containing 180 μmol Metal g_{cat}^{-1}, (a) before activation and (b) after a 'fast activation' for 30 min at 350 °C and (c) 400 °C.
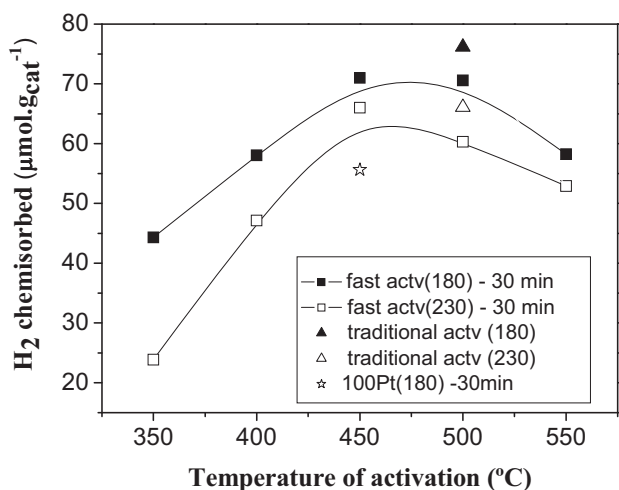
Fig. 9. Amount of hydrogen chemisorbed on the 60Pt/H-BEA catalyst containing 180 and 230 μmol Metal g_{cat}^{-1} as a function of activation conditions.

to the original curve, showing that a large part of the cations was reduced under these conditions. However, the TPR curve produced after the activation at 400 °C shows that all cations were reduced at that temperature. Therefore, despite a quick heating rate, the 'fast activation' process is a very efficient method to reduce nickel and platinum cations, when both ions are present in the same catalyst precursor.

On the other hand, Yoshioka et al. [14] observed through the TPR profiles obtained from the 50Pt/H-USY bimetallic catalyst after its 'fast activation', that only at 500 °C all the cations were reduced. This result shows that in the Pt–Ni/H-BEA catalysts the cations are easier reduced than in the Pt–Ni/H-USY catalysts. This can be explained by the higher accessibility of hydrogen to the cations presents in zeolite Beta due its very small crystallites that promotes rapid hydrogen diffusion.

Fig. 9 shows the amount of hydrogen chemisorbed on 60Pt/H-BEA catalysts reduced by 'fast activation', as well by the 'traditional activation' method. For the catalysts reduced with the 'fast activation' method, the amount of chemisorbed hydrogen at 350 °C was very small, owing to the amount of unreduced cations at this temperature, as shown by TPR analysis (Fig. 8). It can also be seen that as the final temperature is increased up to 450 °C, there is a large increase in the amount of chemisorbed hydrogen. This indicates that, as activation temperature rises, there is an increase in the amount of metal at the surface. This can be explained by two simultaneous factors: an increase in the amount of reduced metal and a decrease in the average diameter of metal particles.

For the catalyst precursors reduced at temperatures above 450 °C, the amount of chemisorbed hydrogen decreases again. As already shown in Fig. 9, the catalyst activated at 400 °C (curve c) has no further reducible cations. Consequently, in the catalysts reduced at temperatures above 450 °C, the decrease in hydrogen chemisorption is probably due to sintering of the metallic particles.

Fig. 9 also shows that the catalyst with higher metallic content (230 μmol Metal g_{cat}^{-1}) adsorbed less hydrogen than that containing 180 μmol Metal g_{cat}^{-1}. This suggests that the specific surface area of metal is lower in the catalyst with higher metal content and explains the lower catalytic activity shown in Figs. 1a and 2. Fig. 9 also shows the hydrogen chemisorption over the monometallic 100Pt/H-BEA catalyst containing 180 μmol Pt g_{cat}^{-1}, reduced by 'fast activation' at 450 °C. It can be seen that the bimetallic 60Pt/H-BEA catalyst, with the same total metal content, chemisorbs more hydrogen than the monometallic 100Pt/H-BEA catalyst. This indicates that, in the bimetallic catalyst, metals are more exposed than

in the platinum monometallic one and explains the higher catalytic activity of 60Pt/H-BEA catalyst (Fig. 2). This also suggests that the addition of Ni possibly enables the formation of more platinum particles or prevents the aggregation of the platinum particles formed during the process of activation.

Fig. 9 further shows that the catalysts activated by the 'traditional' method at 500 °C (indicated by triangles) chemisorbs amounts of hydrogen very close to those achieved with the 'fast activation' method at the same temperature (indicated by squares). This means that the metallic surface areas of these samples are similar and explains their comparable catalytic activity (Fig. 1a). Therefore, these results confirm the advantage of the 'fast activation' method [13,14]: it can produce materials with almost the same catalytic performance, or even superior, in shorter times.

The amounts of chemisorbed hydrogen on the Pt–Ni/H-BEA catalysts (Fig. 9) were significantly higher than the amounts obtained by Yoshioka et al. [14] with Pt–Ni/H-USY catalysts. The maximum value obtained by these authors was 12 μmol H_2 $g_{cat.}^{-1}$. Therefore, it can be concluded that the metallic particles formed on the Beta zeolite in this work are more exposed than in USY zeolite [14].

4. Conclusions

Under the same activation and test conditions, the activities of Pt–Ni/H-BEA catalysts were significantly higher than those of Pt–Ni/H-USY catalysts. Desorption rates of *n*-paraffins from the Beta zeolite were also significantly higher than from the USY zeolite, according to ZLC analysis. These differences are attributed to the much smaller crystallites of the Beta zeolite (20–30 nm), seen by HRTEM analysis, compared to USY zeolite (800 nm). The smaller diffusion path accelerates the transfer of reactants and products. Besides, Beta zeolite nanocrystals enhance the activation of the catalyst, improving the reduction and metal dispersion. The higher activity of Beta catalyst allows the reaction to be run at lower temperatures, resulting in selectivity to isomerization close to 100%.

The 'fast activation' of bimetallic catalysts supported on Beta zeolite was more effective than 'traditional activation': it decreased the activation time and increased the isomerization activity of the catalysts. Highest activity was achieved with catalyst reduced at temperatures between 400 and 450 °C for 30 min. For longer times and higher temperatures of activation, the isomerization activity decreased due to the sintering of metal particles and a consequent reduction of metallic dispersion.

Concerning the percentage of platinum in the catalyst, the activity of Pt–Ni/H-BEA catalyst increased up to 60 mol% Pt and the 60Pt/H-BEA bimetallic catalyst showed better global metallic dispersion than the 100Pt/H-BEA one. This result is very interesting as the bimetallic catalyst costs less than the platinum one.

The highest catalytic activity was achieved with catalysts containing 180 μmol Metal g_{cat}^{-1}, of which 60% was platinum. This activity increase is related to the higher dispersion of the metal particles observed by hydrogen chemisorption analysis. Larger amounts of metal diminish both the metallic dispersion and the catalytic activity.

References

[1] J. Weitkamp, W. Gerhardt, P.A. Jacobs, Acta Phys. Chem. 31 (1985) 31–42.

[2] J. Weitkamp, P.A. Jacobs, J.A. Martens, Appl. Catal. 8 (1983) 123–141.
[3] J. Weitkamp, Stud. Surf. Sci. Catal. 7 (1981) 1404–1405.
[4] M.A. Arribas, F. Márquez, A. Martínez, J. Catal. 190 (2000) 309–319.
[5] E. Furimsky, F.E. Massoth, Catal. Today 52 (1999) 381–495.
[6] A. Corma, Catal. Lett. 22 (1993) 33–52.
[7] Z.B. Wang, A. Kamo, T. Moneda, T. Yashima, Appl. Catal. A: Gen. 159 (1997) 119–132.
[8] A. Chica, A. Corma, J. Catal. 187 (1999) 167–176.
[9] C. Jiménez, F.J. Romero, R. Roldán, J.M. Marinas, J.P. Gómez, Appl. Catal. A: Gen. 249 (2003) 175–185.
[10] R. Roldán, F.J. Romero, C. Jiménez, J.M. Marinas, J.P. Gómez, Appl. Catal. A: Gen. 288 (2005) 104–115.
[11] A. Chica, A. Corma, Chem. Ing. Tech. 79 (2007) 857–870.
[12] M.H. Jordão, V. Simões, D. Cardoso, Appl. Catal. A: Gen. 319 (2007) 1–6.
[13] C.M. Yoshioka, M.H. Jordão, D. Cardoso, Brazil Patent Application PI 0603515-9 (2006).
[14] C.M. Yoshioka, M.H. Jordão, D. Zanchet, T.F. Garetto, D. Cardoso, Appl. Catal. A: Gen. 355 (2009) 20–26.
[15] S. Phatanasri, P. Prasertham, S. Panichsarn, React. Kinet. Catal. Lett. 71 (2000) 281–287.
[16] S. Gopal, P.G. Smirniortis, J. Catal. 225 (2004) 278–287.
[17] G. Brauer, Handbook of Preparative Inorganic Chemistry, Vol. 2, Academic, New York, 1965, pp. 1545–1546.
[18] J.L. Figueiredo, F.R. Ribeiro, Catálise Heterogênea, Fundação Calouste Gulbenkian, 1987, Lisboa, pp. 138–139.
[19] M.H. Jordão, V. Simões, A. Montes, D. Cardoso, Stud. Surf. Sci. Catal. 130C (2000) 2387–2392.
[20] J. Weitkamp, L. Puppe, Catalysis and Zeolite, Fundamentals and Applications, Springer, New York, 1999, pp. 314–315.
[21] M. Guisnet, F.R. Ribeiro, Les Zeolithes, Un nanomonde au Service de la Catalyse, EDP, Les Ulies, 2006, pp. 53–54.
[22] P.M. Lima, C.V. Gonçalves, C.L. Cavalcante Jr., D. Cardoso, Micropor. Mesopor. Mater. 116 (2008) 352–357.
[23] M.M.J. Treacy, J.B. Higgins, Collection of Simulated XRD Powder Patterns of Zeolites, 4 ed., Elsevier, Amsterdam, 1996, pp. 392–393.
[24] M.A. Camblor, A. Corma, S. Valencia, Micropor. Mesopor. Mater. 25 (1998) 59–74.
[25] A. Omegna, M. Vasic, J.A. Van Bokhoven, G. Pirngruber, R. Prins, Phys. Chem. Chem. Phys. 6 (2004) 447–452.
[26] Q.-H. Xia, S.-C. Shenb, J. Songb, S. Kawi, K. Hidajat, J. Catal. 219 (2003) 74–84.
[27] C.L. Cavalcante Jr., N.M. Silva, E.F. Souza-Aguiar, E.V. Sobrinho, Adsorption 9 (2003) 205–212.
[28] R.-M. Jao, T.-B. Lin, J.-R. Chang, J. Catal. 161 (1996) 222–229.
[29] M. Suzuki, K. Tsutsumi, H. Takahashi, Y. Saito, Zeolites 9 (1989) 98–103.
[30] M.S. Tzou, B.K. Teo, W.M.H. Sachtler, J. Catal. 113 (1988) 220–235.
[31] L.-W. Ho, C.-P. Hwang, J.-F. Lee, I. Wang, C.-T. Yeh, J. Mol. Catal. A: Chem. 136 (1998) 293–299.
[32] D.J. Ostgard, L. Kustov, K.R. Poeppelmeier, W.M.H. Sachtler, J. Catal. 133 (1992) 342–357.